






Article

Inositol Phosphoryl Transferase, *Ipt1*, Is a Critical Determinant of Azole Resistance and Virulence Phenotypes in *Candida glabrata*

Garima Shahi ¹, Mohit Kumar ^{1,2}, Nitesh Kumar Khandelwal ³, Atanu Banerjee ¹, Parijat Sarkar ⁴ ,
Sonam Kumari ², Brooke D. Esquivel ⁵ , Neeraj Chauhan ⁶, Amitabha Chattopadhyay ⁴ , Theodore C. White ⁵ ,
Naseem A. Gaur ² , Ashutosh Singh ^{7,*} and Rajendra Prasad ^{1,*}

¹ Amity Institute of Biotechnology and Integrative Science and Health, Amity University Gurgaon, Gurgaon 122412, India; garimashahi47@yahoo.com (G.S.); mohitplawat007@gmail.com (M.K.); atanuj83@gmail.com (A.B.)

² Yeast Biofuel Group, International Centre for Genetic Engineering and Biotechnology, New Delhi 110067, India; sonamverma.sv85@gmail.com (S.K.); naseem@icgeb.res.in (N.A.G.)

³ Department of Chemistry and Biochemistry, University of Arizona, Tucson, AZ 85721, USA; nitesh.k.khandelwal@gmail.com

⁴ CSIR-Centre for Cellular and Molecular Biology, Uppal Road, Hyderabad 500007, India; parijat@ccmb.res.in (P.S.); amit@ccmb.res.in (A.C.)

⁵ School of Biological and Chemical Sciences, University of Missouri at Kansas City, Kansas City, MO 64110, USA; bdp3k9@mail.umkc.edu (B.D.E.); whitetc@umkc.edu (T.C.W.)

⁶ Department of Microbiology, Biochemistry and Molecular Genetics, New Jersey Medical School, Rutgers, The State University of New Jersey, Newark, NJ 07103, USA; chauhan1@njms.rutgers.edu

⁷ Department of Biochemistry, University of Lucknow, Lucknow 226007, India

* Correspondence: ashutosh.singh29@gmail.com (A.S.); rprasad@ggn.amity.edu (R.P.)



Citation: Shahi, G.; Kumar, M.; Khandelwal, N.K.; Banerjee, A.; Sarkar, P.; Kumari, S.; Esquivel, B.D.; Chauhan, N.; Chattopadhyay, A.; White, T.C.; et al. Inositol Phosphoryl Transferase, *Ipt1*, Is a Critical Determinant of Azole Resistance and Virulence Phenotypes in *Candida glabrata*. *J. Fungi* **2022**, *8*, 651. <https://doi.org/10.3390/jof8070651>

Academic Editor: David S. Perlin

Received: 1 June 2022

Accepted: 18 June 2022

Published: 21 June 2022

Publisher's Note: MDPI stays neutral with regard to jurisdictional claims in published maps and institutional affiliations.



Copyright: © 2022 by the authors. Licensee MDPI, Basel, Switzerland. This article is an open access article distributed under the terms and conditions of the Creative Commons Attribution (CC BY) license (<https://creativecommons.org/licenses/by/4.0/>).

Abstract: In this study, we have specifically blocked a key step of sphingolipid (SL) biosynthesis in *Candida glabrata* by disruption of the orthologs of ScIpt1 and ScSkn1. Based on their close homology with *S. cerevisiae* counterparts, the proteins are predicted to catalyze the addition of a phosphorylinositol group onto mannosyl inositolphosphoryl ceramide (MIPC) to form mannosyl diinositolphosphoryl ceramide (M(IP)₂C), which accounts for the majority of complex SL structures in *S. cerevisiae* membranes. High throughput lipidome analysis confirmed the accumulation of MIPC structures in $\Delta Cgip1$ and $\Delta Cgskn1$ cells, albeit to lesser extent in the latter. Noticeably, $\Delta Cgip1$ cells showed an increased susceptibility to azoles; however, $\Delta Cgskn1$ cells showed no significant changes in the drug susceptibility profiles. Interestingly, the azole susceptible phenotype of $\Delta Cgip1$ cells seems to be independent of the ergosterol content. $\Delta Cgip1$ cells displayed altered lipid homeostasis, increased membrane fluidity as well as high diffusion of radiolabeled fluconazole (³H-FLC), which could together influence the azole susceptibility of *C. glabrata*. Furthermore, in vivo experiments also confirmed compromised virulence of the $\Delta Cgip1$ strain. Contrarily, specific functions of CgSkn1 remain unclear.

Keywords: *Candida glabrata*; sphingolipids; inositolphosphorylceramide; lipidomics; drug resistance; virulence

1. Introduction

Pathogenic fungi can develop clinical drug resistance after persistent drug exposure, which may impede successful treatment of human infections [1]. The most common human pathogenic fungi, *Candida albicans* and non *albicans Candida* (NAC) species, possess a repertoire of mechanisms to defy toxicity from multiple drugs. Among the various mechanisms of drug resistance, rapid drug efflux accomplished by select transporters stands out as the most prevalent mechanism of resistance [2]. Several factors have been

identified that contribute to the fungal cellular responses to drugs, and antifungal resistance in *Candida* species is a complex multifactorial process.

Notably, several antifungal drugs target enzymes involved in lipid biosynthesis in *Candida* species. There is also a proven intricate relationship between membrane lipid homeostasis, micro-viscosity and drug resistance in *Candida* species [3,4]. For example, changes in membrane lipid phase and asymmetry affect azole resistance [5]. Any imbalances among membrane micro-domain (membrane raft) constituents lead to protein sorting defects and impacts on drug susceptibility in *C. albicans* [6]. Additionally, perturbation associated with phosphoglyceride (PGL) or sphingolipid (SL) metabolism also influences drug susceptibility, irrespective of whether a drug targets lipids or other cellular components [6,7]. Together, the drug susceptibility phenotype of *Candida* species appears to result from an orchestrated interplay between intracellular drug accumulation, drug efflux and the membrane lipid environment. The role of lipids is not restricted to drug resistance; and impacts a variety of cellular processes including biofilm formation and virulence [8,9]. Notably, certain SL structures are unique to fungi, which, apart from being novel drug targets, also appear to act as molecular signals, manifesting roles in diverse biological processes [10–16]. Independent observations from others and our group have revealed that in *C. albicans*, a complex relationship between SL and ergosterol homeostasis exists which has repercussions on virulence and susceptibility to antifungals [17–21]. For instance, an intermediate of SL metabolism, glucosylceramide, has been identified as a novel virulence factor in *C. albicans* and ceramide synthase as a virulence factor in encapsulated yeast *Cryptococcus neoformans* [22].

C. glabrata infection incidences stand out as the second most common NAC in hospitals [23], and reports state that *C. glabrata* is intrinsically less susceptible to azole antifungal with a mortality rate of 50% in patients with invasive infections [24–26]. Several studies have been done to understand the resistance mechanism of *C. glabrata* among which increased drug efflux due to upregulation of efflux pump is the main described mechanism, which is caused by gain-of-function (GoF) mutation in *CgPDR1*, a transcriptional regulator of drug resistance [27–36]. Higher adherence and high number of adhesins which are encoded by EPA family genes is crucial for the pathogenicity of *C. glabrata* as well [37]. Unlike other *Candida* species, *C. glabrata* cannot form true hypha so the phenotypic conversion to hyphal growth, which is an important virulence mechanism, is missing; however, *C. glabrata* has a completely different way of coping up with macrophage mediated phagocytosis. Following the engulfment by the macrophages, *C. glabrata* cells are somehow able to survive for a longer period of time and continue to divide [38].

In this study, we have specifically attempted to block the key synthesis step of SL metabolism by deleting the genes encoding *CgIpt1* and *CgSkn1*, which based on their close homology with *S. cerevisiae* are predicted to be inositolphosphoryl transferases mediating the conversion of mannosyl inositolphosphoryl ceramide (MIPC) to mannosyl diinositolphosphoryl ceramide (M(IP)₂C). We have elucidated the functionality of sphingolipids in *C. glabrata* by blocking the synthesis of M(IP)₂C in $\Delta Cgipt1$ cells leading to enhanced susceptibility to azoles.

2. Materials and Methods

2.1. Strains and Chemicals

C. glabrata strain BG2 referred to as wild type was gifted by Dr. Rupinder Kaur's lab of fungal pathogenesis, CDFD, Hyderabad, India. Strains used in this study are listed in Table S1. Yeast cultures were maintained in YPD broth (2% peptone, 1% yeast extract, 2% glucose) and YPD agar (YPD broth with 2% agar), unless otherwise stated. All the antifungal drugs used in this study were of analytical grade and were procured from Sigma Aldrich, Bangalore, India.

2.2. Deletion and Revertant Construction Strategy

Based on 18S rRNA sequence, *C. glabrata* is evolutionarily more closely related to the non-pathogenic yeast *S. cerevisiae* [39] than to the pathogenic yeast *C. albicans*. Based on the sequence homology of *Ipt1* and *Skn1* with *S. cerevisiae*, deletion mutants of *CgIpt1* and *CgSkn1* were constructed in a wild type (WT) haploid *C. glabrata* BG2 by employing NAT (Nourseothricin acetyltransferase) cassette as per our earlier established protocol [40]. The resulting knockouts were designated as $\Delta Cgipt1$ and $\Delta Cgskn1$.

The revertant strain of $\Delta Cgipt1$ was constructed by the episomal expression of the deleted gene. For revertant construction, a modified plasmid pGRB2.3_HphB was used, which was constructed by replacing the *URA3* gene with the HphB (for hygromycin resistance) selection marker. The GOI ORF was cloned in the pGRB2.3_HphB under its own promoter using Gibson assembly. Clones were verified by bacterial colony PCR and restriction digestion with specific enzymes. The resulting revertant was designated as $\Delta Cgipt1::IPT1$.

2.3. Lipid Extraction

Extractions of lipids were done as per Folch's protocol described previously [41]. Briefly, an overnight culture was inoculated into 50 mL YPD broth to 0.2 OD₆₀₀, grown for 6 h at 30 °C and was disrupted using glass beads. Supernatant was taken in a glass tube and lipids were extracted using a chloroform: methanol (2:1 v/v) ratio. Lipids extracted were dried with the help of an N₂ flush and kept at −20 °C for further analysis. Dry weights of the extracted lipids were recorded at this point for the normalization of mass spectral data.

2.4. Mass Spectrometry Analysis

Lipid extracts were dissolved in 1 mL chloroform. To the 2–3 µL aliquots of these dissolved lipids, internal standards were added as described previously [42]. Lipid extracts were then analyzed on a Xevo TQ-XS triple quadrupole mass spectrometer (XEVO-TQS#WAA627, Waters, UK; Milford, MA, USA). Various lipid classes and individual molecular lipid species were determined using the neutral loss, negative and positive multiple precursor ion scans as described earlier [7,42,43]. Data processing was performed using the TargetLynx XS™ software (Waters, UK; Milford, MA, USA) and data was normalized to lipid dry weight and represented as nmol/mg lipid dry weight.

2.5. Gas Chromatography Mass Spectrometry (GCMS)

For free sterol analysis, base hydrolyzed lipid extract was derivatized with N, O-Bis (trimethylsilyl) trifluoroacetamide with trimethyl-chlorosilane (BSTFA/TMCS, Sigma, St. Louis, MO, USA) and analyzed on DB5-MS column (30 m × 0.2 mm × 0.20 µm) as described previously [43]. The retention time and mass spectral patterns of external standards were used for identification of sterol species.

2.6. Growth Assay

The growth kinetics was performed by a micro-cultivation method in a 96-well plate using a Liquid Handling System (Tecan, Austria) in YPD broth at 30 °C as described previously [40]. Briefly, overnight grown yeast cultures were diluted to 1.0 OD₆₀₀ and 20 µL of each culture was mixed with 180 µL YPD broth in the 96-well plate. Different volumes of drugs, according to their indicated concentration, were added to the wells. The OD₆₀₀ was measured at 30 min intervals up to 24 h.

2.7. Minimal Inhibitory Concentration (MIC) Measurements

The MICs for the strains were determined by the broth micro dilution method as described earlier [44]. Briefly, cells were grown for 12–14 h at 30 °C to obtain single colonies. They were then resuspended in a 0.9% normal saline solution to give an OD₆₀₀ of 0.1. The cells were then diluted 100-fold in YPD medium. The diluted cell suspension was added to the wells of round-bottomed 96-well microtiter plates containing equal volumes of medium

and different concentrations of drugs. A drug-free control was also included. The plates were then incubated at 30 °C for 24 h. The MIC test end point was evaluated by reading the OD₆₀₀ in a microplate reader and was defined as the lowest drug concentration that gave 80% inhibition of growth compared with the growth of the drug-free control.

2.8. Spot Microdilution Assay

Samples of fivefold serial dilutions of each culture, each with cells suspended in normal saline to an OD₆₀₀ of 0.1 were spotted onto YPD plates in the absence (control) or in the presence of drugs as described earlier [3]. Growth differences were recorded following incubation of the plates for 24 h at 30 °C.

2.9. Uptake Measurements of Radiolabelled ³H-FLC

The ³H-FLC accumulation assay was performed as described previously [45]. Overnight-grown (16 h shaking cultures in YPD medium at 30 °C) samples were washed three times with YNB (yeast nitrogen base), starved of glucose for 3 h, and then treated with ³H-FLC in YNB ± 2% glucose in technical duplicate. Samples were incubated with shaking at room temperature over the course of 3, 8 and 24 h. Previous azole import analyses have revealed that most fungal cells reach maximum intracellular drug accumulation by 24 h [46,47], so no measurements were taken after the 24 h time point. At each time point, the OD₅₉₅ of each sample was taken, and then a stop solution, consisting of YNB + FLC (20 mM), was mixed with each sample. Then samples were poured over glass microfiber filters on a vacuum and washed again with 5 mL YNB. Filters with washed cells were placed in scintillation fluid and the radioactivity was measured in a Beckman Coulter LS 6500 Scintillation Counter. Values were adjusted to CPM per 10⁸ cells based on the OD₅₉₅ of each sample recorded right before filtering.

2.10. Fluorescence Imaging and FRAP (Fluorescence Recovery after Photobleaching)

C. glabrata staining with FAST-DiI was performed as described previously [17]. *C. glabrata* culture was suspended at a density of 10⁸ cells/mL in 1 M sorbitol-0.1 M EDTA buffer and labelled using a final concentration of 10 µM FAST-DiI. Confocal imaging was carried out on an inverted Zeiss LSM 510 Meta confocal microscope using the 561 nm laser and fluorescence emission was collected using the 575–630 nm bandpass filter. Diffusion coefficient (D) and mobile fraction (M_f) were calculated from quantitative FRAP experiments. FRAP experiments were performed with Gaussian spot-photobleaching and line-scanning mode with circular ROI of 1 µm radius. Data representing the mean fluorescence intensity in the membrane region within the bleach spot were corrected for background and analyzed. Non-linear curve fitting was used to analyze the fluorescence recovery plot and the graph was plotted using GraphPad Prism. Fluorescence recovery profiles and diffusion coefficients were analyzed as described by Koppel et al. [48].

2.11. Virulence Study

For virulence experiment, we used neutropenic murine model of systemic candidiasis [49]. To induce neutropenia, BALB/c mice were injected with 200 mg/kg intraperitoneal (ip) cyclophosphamide and subcutaneous cortisone acetate three days prior to the beginning of the experiment. *C. glabrata* WT, Δ *Cgip1* and Δ *Cgip1::IPT1* strains were grown in YPD broth at 30 °C overnight. Cells were then harvested, washed, and suspended in PBS to a required density. In BALB/c mice, strains were injected once via the lateral tail vein with 100 µL suspension containing 5 × 10⁵ *C. glabrata* cells. Mice were euthanized at 48 h post-infection. Kidneys were harvested and enumerated for *C. glabrata* burdens.

3. Results

3.1. The Deletion of *CgIpt1* and *CgSkn1* in *Candida Glabrata*

Based on the close homology with *S. cerevisiae*, the two ORFs, CAGL0G05313g and CAGL0I10054g of the SL biosynthetic pathway of *C. glabrata*, showed 51.51% and 61.76% sequence similarity in their protein sequences with ScIpt1 and ScSkn1, respectively. Both open reading frames (ORFs) were deleted individually in *C. glabrata* by employing a fusion-based PCR method and deletants were confirmed by semiquantitative PCR as described earlier [40]. Viable colonies obtained after single deletion of the *CgIpt1* and *CgSkn1* genes confirmed their non-essential nature. Both $\Delta Cgipt1$ and $\Delta Cgskn1$ mutant cells continued to grow on YPD liquid and solid media like wild type (WT) cells, implying that their deletion did not result in any change in cell fitness (data not shown).

3.2. Lipidomics of $\Delta Cgipt1$ and $\Delta Cgskn1$ Mutants Confirmed Their Involvement in SL Metabolism in *C. glabrata*

Inositol phosphoryl transferases have been shown to be the key enzyme in the formation of M(IP)₂C, an abundant complex SL structure in the plasma membrane, reported in *S. cerevisiae* [50]. We analyzed the impact of its deletion in *C. glabrata* cells. For this we performed a comparative profiling of lipids extracted from $\Delta Cgipt1$ and $\Delta Cgskn1$ cells by employing high throughput MS-based lipidomic analysis to establish their role in SL metabolism and if its deletion has any repercussions on the overall lipid homeostasis. Our analysis detected all major PGL classes (lysophosphatidylcholine (LPC), phosphatidylcholine (PC), lysophosphatidylethanolamine (LPE), phosphatidylethanolamine (PE), Phosphatidylinositol (PI), phosphatidylserine (PS), phosphatidic acid (PA) and phosphatidylglycerol (PG)), sphingolipid class compositions (Inositolphosphorylceramide (IPC) and Mannosylinositolphosphorylceramide (MIPC)), ergosterol esters and neutral lipids (DAGs and TAGs).

There were no significant changes observed among the different PGL classes in $\Delta Cgipt1$ and $\Delta Cgskn1$ when compared to the WT (Figure 1A). Our analysis expectedly detected significantly higher amounts of total SLs (as much as 1.8-fold) in $\Delta Cgipt1$ and $\Delta Cgskn1$ cells (Figure 2A–D, Supplementary Sheet S1). The total content of ergosteryl esters also showed increased levels (as much as 12.8-fold) in $\Delta Cgipt1$ and $\Delta Cgskn1$ cells (Figure 2E,F, Supplementary Sheet S1). A 7.3-fold accumulation of the SL's biosynthetic intermediate MIPC in $\Delta Cgipt1$ and 1.6-fold accumulation of $\Delta Cgskn1$ cells confirmed their role in SL metabolism as inositol phosphoryl transferases (Figure 2A–D).

We were able to detect 246 molecular lipid species spanning across 14 different classes of lipids and observed significant variations among several of them in $\Delta Cgipt1$ and $\Delta Cgskn1$ cells. We observed significant variations in PGL species contents of these mutants. For example, molecular species of LPC (LPC14:1 and LPC17:0), PC (PC26:1, PC26:0, PC28:1, PC28:0, PC30:2, PC31:1, PC33:2, PC33:1, PC33:0, PC36:1 and PC38:2), PE (PE26:0, PE33:2, PE34:3, PE35:2, PE35:1 and PE37:1) and PI30:1 species were seen to be reduced in $\Delta Cgipt1$ and $\Delta Cgskn1$ cells; while the level of a few species of PGL classes (PE36:2, PI36:2, PS30:0, PG32:2 and PG34:0) were in abundance in $\Delta Cgipt1$ and $\Delta Cgskn1$ cells (Figure 1B, Supplementary Sheet S1). The SL species IPC46:0–2, MIPC44:0–2, MIPC44:0–3, MIPC46:0–2 and MIPC46:0–3 were abundant in $\Delta Cgipt1$ cells (Figure 2B,D).

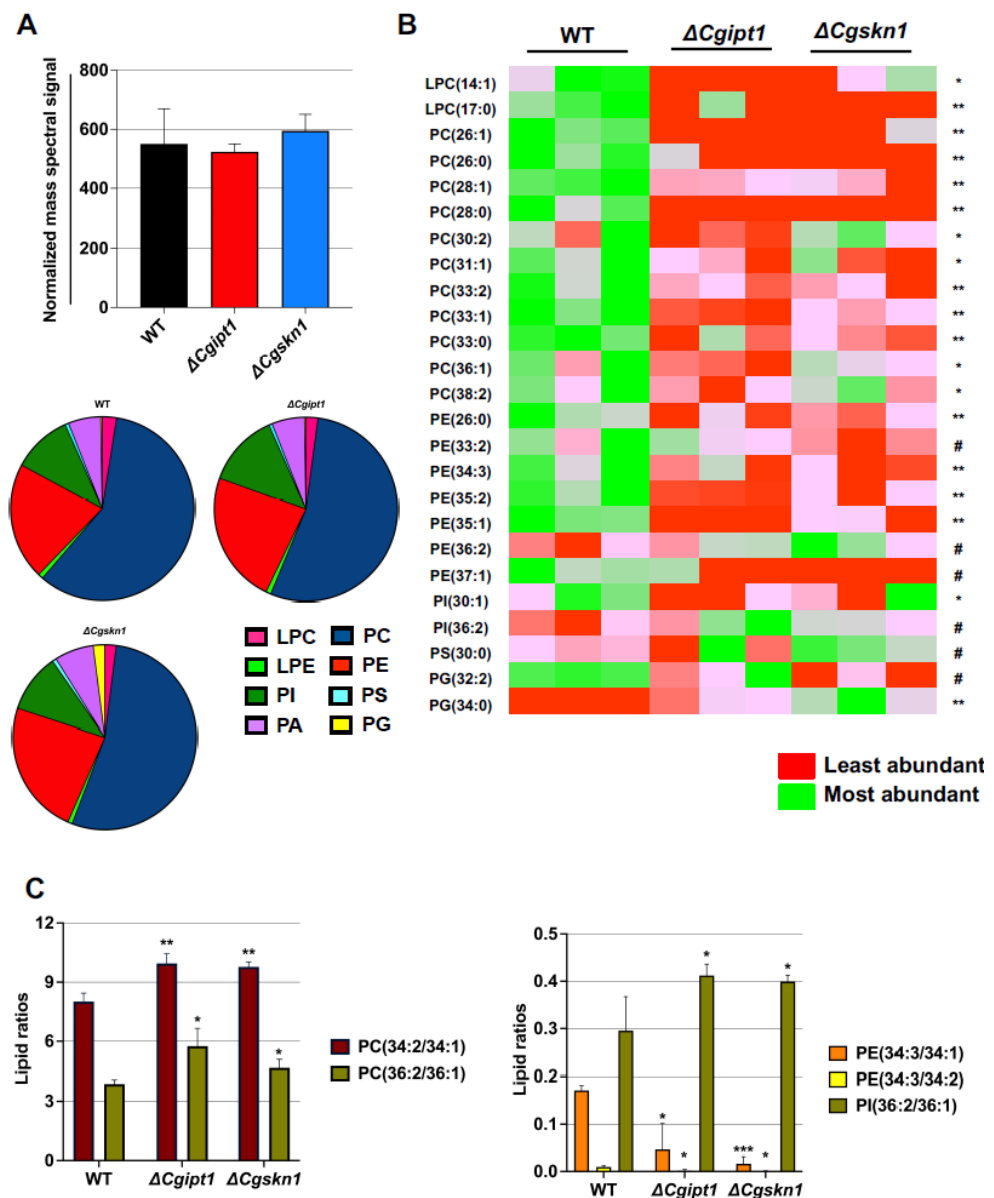


Figure 1. Lipidomic analysis reveals significant changes in PGL species in $\Delta Cgipt1$ and $\Delta Cgskn1$ mutants of *C. glabrata*. (A) The total PGL content, along with the content of specific PGL classes of PC, LPC, PE, LPE, PI, PS, PG and PA, in WT, $\Delta Cgipt1$ and $\Delta Cgskn1$ mutants of *C. glabrata* are depicted. (B) Compared to the WT, $\Delta Cgipt1$ and $\Delta Cgskn1$ mutants of *C. glabrata* show significant changes in PGL molecular species compositions. The PGL species are represented as “total number of carbons in the acyl chains: total number of carbon-carbon double bonds in the acyl chains”. Data represents nmol per mg lipid dry wt. as total normalized mass spectral signal and can be found in supplementary sheet S1. Mean \pm SD of three replicates is plotted. Significant changes in PGL species with a *p*-value of <0.05 are represented by * (WT versus $\Delta Cgipt1$), # (WT versus $\Delta Cgskn1$), and ** (WT versus $\Delta Cgipt1$ and $\Delta Cgskn1$). (C) Variations in the ratio of lipid species between WT vs. $\Delta Cgipt1$ and WT vs. $\Delta Cgskn1$ are shown. Data are represented as mean \pm SEM of three independent replicates. Significant differences from WT ratios with a * *p* value ≤ 0.05 ; ** *p* value ≤ 0.006 ; *** *p* value ≤ 0.0001 calculated using unpaired student’s *t*-test.

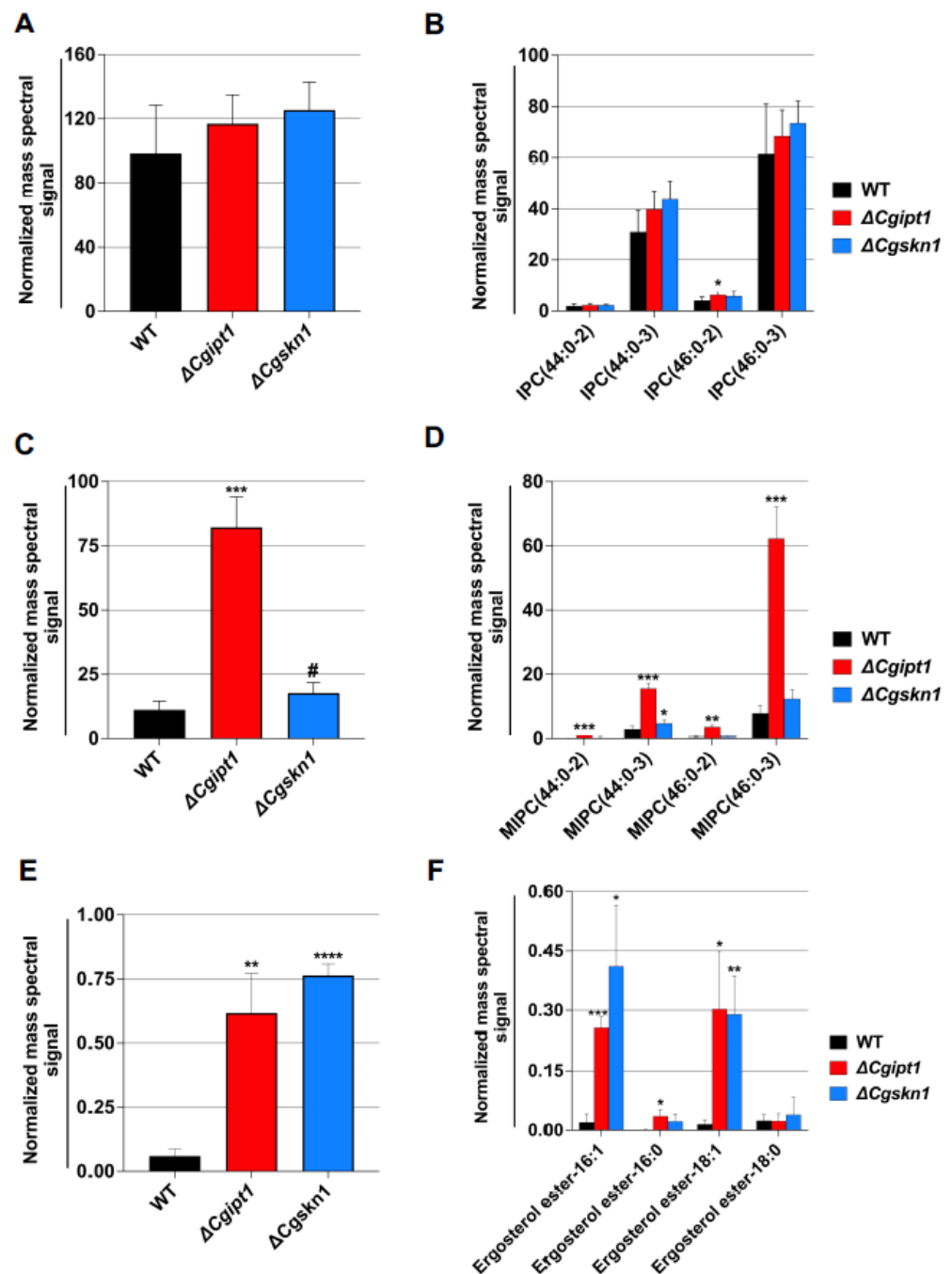


Figure 2. Alterations in SL and ergosteryl ester contents $\Delta Cgipt1$ and $\Delta Cgskn1$ mutants of *C. glabrata*. (A) Total IPC content. (B) IPC species content. (C) Total MIPC content. (D) MIPC species content. (E) Total ergosteryl ester content. (F) Ergosteryl ester species content. IPC and MIPC species are represented as “total number of carbons in the sphingoid base and acyl chains: total number of carbon-carbon double bonds in the sphingoid base and acyl chains- number of hydroxyl groups present in the sphingoid base and acyl chains”. Data represents nmol per mg lipid dry wt as total normalized mass spectral signal and can be found in Supplementary Sheet S1. Mean \pm SD of three replicates is plotted and compared to WT. * p value ≤ 0.05 ; ** p value ≤ 0.007 ; *** p value ≤ 0.0008 ; **** p value < 0.0001 ; # p value 0.10 were calculated using unpaired student’s t test.

3.3. *CgSkn1* Does Not Significantly Impact MIPC Metabolism

The role of *Skn1* in SL metabolism in yeasts remains unclear. Independent studies have reported that *ScSkn1*, a homologue of *ScIpt1* in yeast, is involved in the biosynthesis of $M(IP)_2C$. For instance, $\Delta Scskn1$ and $\Delta Scipt1$ single and double deletion mutants of *S. cerevisiae* cells, when grown in a nutrient-rich medium, show a complete absence of $M(IP)_2C$ and thus confirm the role of *ScSkn1* in MIPC metabolism [51]. Correspondingly, the other roles of *Skn1* such as regulating β -1,6-glucan synthesis, hyphal and biofilm development, autophagy and virulence are also highlighted [50,52–55]. *CaSkn1* role in the virulence of *C. albicans* is well demonstrated where its deletion along with another homologue, *CaKre6*, involved in glycan biosynthesis, results in attenuated virulence [54]. In the present study, we explored the role of *Skn1* of *C. glabrata* in the biosynthesis of $M(IP)_2C$. Our high throughput lipidomic analysis of $\Delta Cgskn1$ cells and its comparison with $\Delta Cgipt1$ cells showed that the deletion of the gene-encoding *CgSkn1* did not cause any major changes in SL metabolism. Our data showed no significant changes in total SLs and its classes when compared with the WT cells, and in contrast to $\Delta Cgipt1$ cells, relatively less accumulation of MIPC was detected in $\Delta Cgskn1$ cells (Figure 2D). This further confirms that *CgSkn1*, unlike its counterpart in *S. cerevisiae*, may not be a major contributor in MIPC metabolism in *C. glabrata*; however, a supporting role is suspected.

3.4. $\Delta Cgipt1$ Cells Manifest Increased Drug Susceptibility

Both $\Delta Cgipt1$ and $\Delta Cgskn1$ cells were subjected to detailed drug susceptibility and phenotypic tests by employing three independent methods i.e., growth assay, minimal inhibitory concentration (MIC) and spot assays (Figure 3, Figure S1 and Figure S2). Interestingly, we noticed that the accumulation of MIPC in $\Delta Cgipt1$ cells was accompanied by raised susceptibility towards azoles (Figure 3A,B). $\Delta Cgipt1$ showed increased susceptibility to both imidazoles (KTZ, MCZ and CTZ) and triazoles (FLC, ITR, PCZ) (Figure S1A).

However, the $\Delta Cgipt1$ strain displayed no change in susceptibility towards a range of various other tested compounds like Congo red (CR), caffeine (CAF), calcofluor white (CFW), cycloheximide (CHX), verapamil (VER), o-phenanthroline (OP), 4-nitroquinoline (4NQO), chloramphenicol (CHL), acetic acid (AcOH; pH 4.5), anisomycin (ANM), naftifine (NAFT), myriocin (MYR), terbinafine (TRB) and hydrogen peroxide (H_2O_2) (Figure S1B). The growth of $\Delta Cgipt1$ cells in comparison to parent cells on solid agar media also remain unaffected at different temperatures, pHs, carbon sources and iron chelators (Figure S1B).

In contrast to $\Delta Cgipt1$ cells, the deletant $\Delta Cgskn1$ did not manifest any change in drug susceptibility (Figure S2). However, the double deletion mutant, $Cgipt1/Cgskn1\Delta\Delta$, expectedly showed increased susceptibility towards azoles caused by the absence of functional *CgIpt1* in $Cgipt1/Cgskn1\Delta\Delta$ cells (Figure 3C). Since $\Delta Cgskn1$ cells did not display significant changes in SL metabolism and in drug susceptibility, we did not include it in our further experiments.

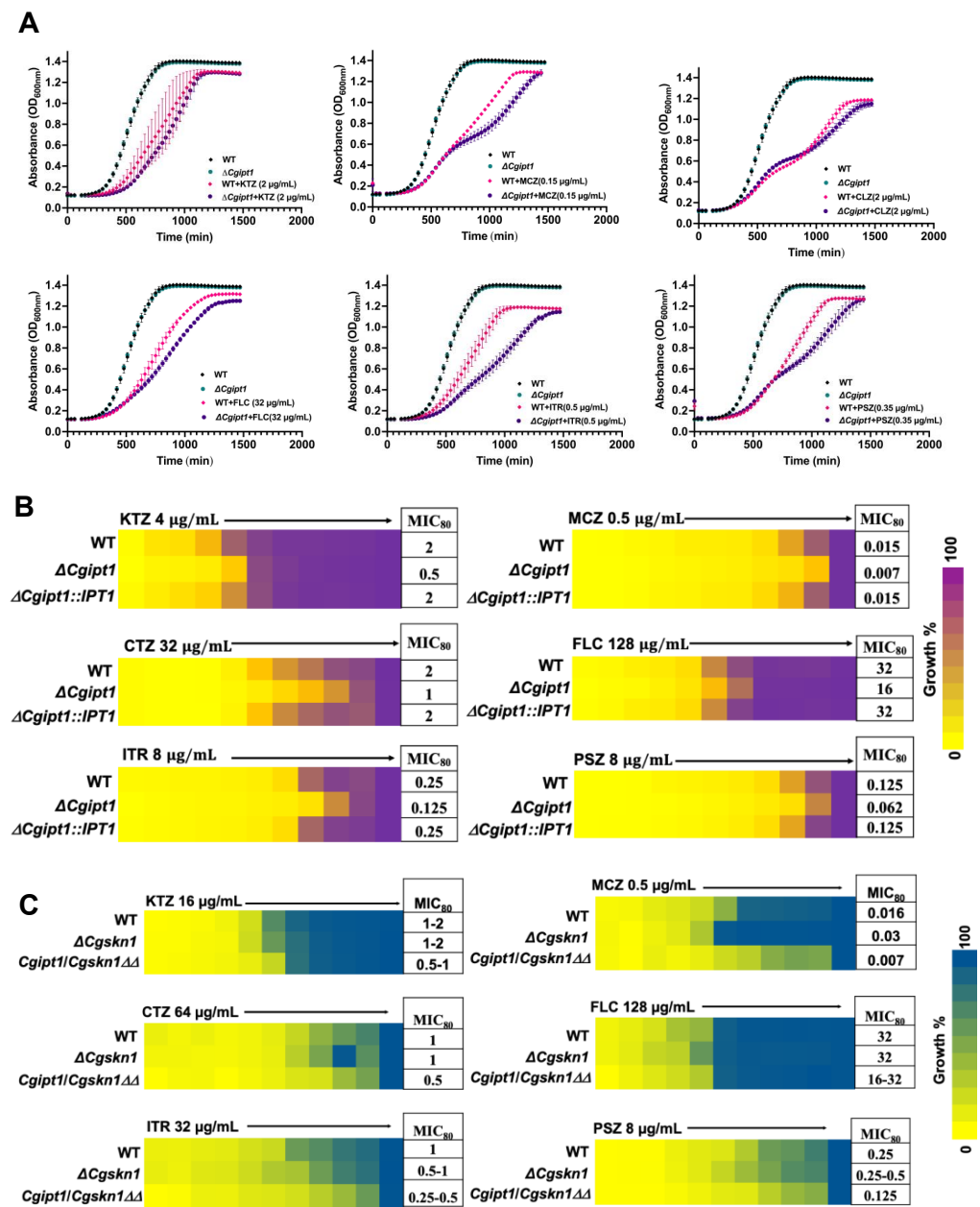


Figure 3. Drug susceptibility analysis of $\Delta Cgipt1$, $\Delta Cgskn1$ and $Cgipt1/Cgskn1 \Delta\Delta$ mutants of *C. glabrata*. Drug susceptibility to KTZ, MCZ, CTZ, FLC, ITR and PCZ was determined by (A) growth curve analysis, (B,C) broth microdilution assay as described in our earlier publications and briefly mentioned in Section 2.

3.5. $\Delta Cgipt1$ Cells Revealed Increase Levels of Sterols

From our lipidomic analyses, we recorded an increase in the total ergosteryl esters as well as their species in $\Delta Cgipt1$ cells (Figure 2E,F). Following this we checked the total sterol and their species content in $\Delta Cgipt1$ by employing GC-MS. Our GC-MS analysis could detect eight different sterol species, namely squalene, dehydroergosterol, ergosterol, fecosterol, episterol, fungisterol, lanosterol and UI-sterol. The content of total sterol and their intermediates was significantly higher in $\Delta Cgipt1$ cells compared to WT cells (Figure 4A,B). Among these, ergosterol and squalene were the most abundant lipids detected. It appears that $\Delta Cgipt1$ cells tend to accumulate free sterols in response to the depletion of $M(IP)_2C$ as a compensatory mechanism for the loss of complex SLs (See Section 4).

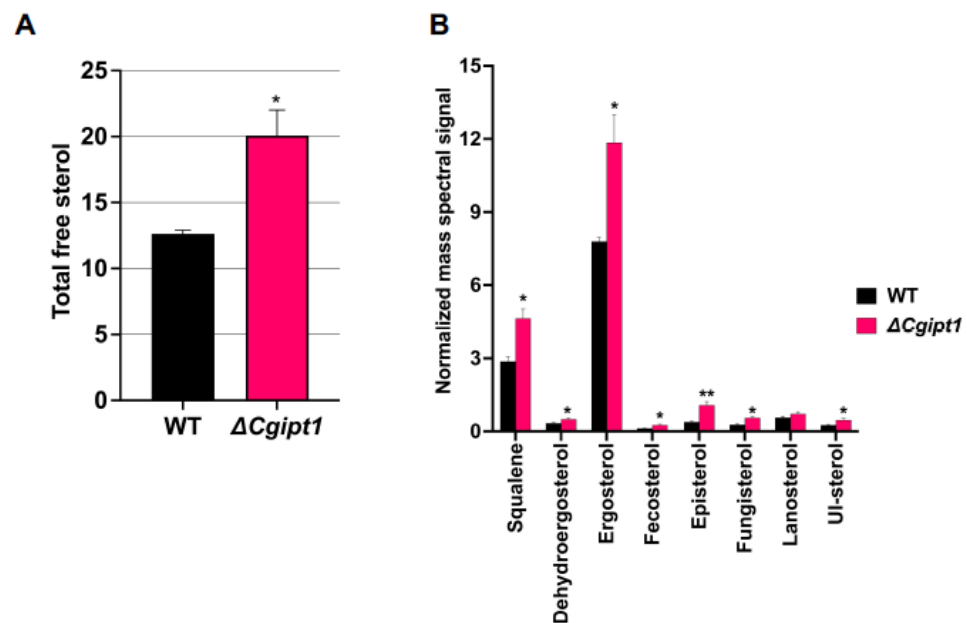


Figure 4. Deletion of *CgIpt1* perturbs the sterol homeostasis in *C. glabrata*. (A) Total free sterol content. (B) Content of different sterol species detected by GCMS. Mean \pm SD of five replicates is plotted. * p -values < 0.05; ** p -values < 0.009 calculated using unpaired student's t test.

3.6. Deletion of *CgIpt1* Leads to Reduced PM Rigidity

Since drug diffusion and susceptibility of *Candida* cells has been linked to the physical state of the PM earlier [3,17,56,57], we explored if changes in MIPC levels observed in $\Delta CgIpt1$ cells could alter the permeability of the PM. For measuring membrane fluidity changes in $\Delta CgIpt1$ cells, we employed FRAP analysis by using the dye FAST-DiI as described in Materials and Methods. Both WT and $\Delta CgIpt1$ cells were photobleached and the region was imaged over time to check the recovery of the dye fluorescence. Figure 5A depicts the representative fluorescence recovery experiment images of WT and $\Delta CgIpt1$ strains. As shown in the overlapping recovery plot, $\Delta CgIpt1$ cells showed faster recovery of the dye fluorescence to the bleached area as compared to the WT strain (Figure 5B).

Analysis of fluorescence recovery plots showed that $\Delta CgIpt1$ mutant cells indeed showed a higher diffusion coefficient value ($3.84 \times 10^{-9} \text{ cm}^2/\text{s}$) as compared to the WT strain that showed a lower diffusion coefficient value ($0.84 \times 10^{-9} \text{ cm}^2/\text{s}$) (Figure 5C). Further, we calculated the mobile fraction as described in Materials and Methods. Along with higher diffusion coefficient values, we also observed higher mobile fraction of the dye in $\Delta CgIpt1$ cells (58.35%) when compared with WT cells (40.74%) (Figure 5D). These results confirmed a higher extent of recovery (mobile fraction) and rate of recovery (diffusion coefficient) in $\Delta CgIpt1$ cells relative to WT cells. Together, we conclude that M(IP)₂C in $\Delta CgIpt1$ cells are essential to maintain optimum viscosity of PM and its absence tends to make the PM more fluid.

Changes in lipid ratio compositions can be a good indicator of alterations in membrane fluidity. A closer look at the PGL molecular species showed significant changes in lipid ratios. For instance, the PC34:2/PC34:1 and PC36:2/PC36:1 ratio was higher in $\Delta CgIpt1$ when compared with WT (Figure 1C). Increase in unsaturation index of these lipid ratios correlates with loss of plasma membrane rigidity in $\Delta CgIpt1$ cells (discussed later). It is reported that imbalances in PE levels influence the viscosity of the plasma membrane bilayer where an increase in PE content leads to increased rigidity of the membrane [58]. In the present case, $\Delta CgIpt1$ cells show reduced ratios of PE34:3/34:1 and PE34:3/34:2 (Figure 1C) which implies that the reduction of PE species as well as their lipid ratios in $\Delta CgIpt1$ cells contribute to increased plasma membrane fluidity in these cells. Of note, the amounts of the individual PGL species might not always change between the WT and the deletion strains, however, significant variations could be still observed upon

comparing the PGL species ratios, effecting overall membrane homeostasis. Total contents of saturated FA containing PGLs and odd chain FA containing PGLs were significantly reduced in $\Delta Cgip1$ cells as compared to WT cells (Supplementary Sheet S1). The principal component analysis (PCA) could further validate the statistically significant changes in molecular lipid species between WT and $\Delta Cgip1$ cells (Figure S3). No significant change was seen in the total diacylglycerol (DAG) and triacylglycerol (TAG) contents in $\Delta Cgip1$ (Supplementary Sheet S1) strain.

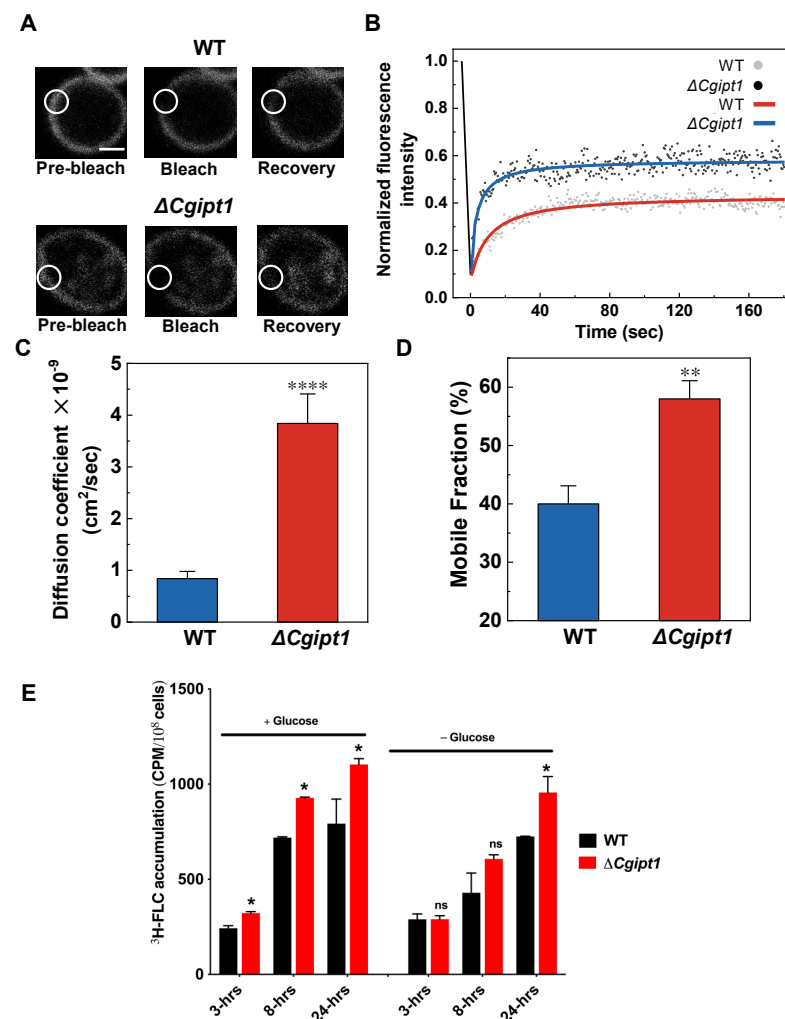


Figure 5. Disruption of CgIpt1 causes reduced PM rigidity. (A) Representative images of FAST-Dil dye-labeled plasma membrane of WT and $\Delta Cgip1$ cells (left column, $t = 0$ s, pre-bleach). A region of interest (ROI, white circle) was photobleached and cells were imaged immediately thereafter (second column, ‘bleach’) and after 180 s post-bleach (third column, ‘recovery’). (B) Overlapped fluorescence recovery curves showing faster recovery in $\Delta Cgip1$ cells relative to WT cells. (C) Diffusion coefficients (D) and mobile fraction (M_f) were calculated for WT and $\Delta Cgip1$ cells. Experiments were performed in biological triplicates and statistical significance values ($p < 0.0001$ (****); $p < 0.0014$ (**)) were calculated using unpaired Student’s *t*-test. (E) $^3\text{H-FLC}$ accumulation in the WT and $\Delta Cgip1$ strains in energized (+Glucose) and deenergized (–Glucose) conditions. Significant differences in FLC accumulation between WT and $\Delta Cgip1$ were calculated and the *p*-values of <0.05 are represented by *; ns, not significantly different.

3.7. $\Delta Cgip1$ Cells Show Enhanced Diffusion of $^3\text{H-FLC}$

It is now well established that entry of azoles into *Candida* species and other pathogenic fungi is predominantly through facilitated diffusion. Increased antifungal drug uptake and accumulation by fungi could lead to increased drug susceptibility, while reduced

drug accumulation could result in resistance to the drug [46,47,59,60]. We investigated whether increased FLC diffusion/accumulation could explain the increased fluconazole susceptibility of $\Delta Cgip1$ cells. We monitored FLC entry by measuring the intracellular accumulation of radiolabeled fluconazole (^3H -FLC) over time as explained earlier [45]. Briefly, $\Delta Cgip1$ and WT cells were treated with ^3H -FLC with and cell samples were withdrawn at the indicated time interval and the intracellular FLC was measured. The assay was performed in both energized (2% glucose) and deenergized (glucose starved) conditions to gain an indication of drug accumulation in actively dividing cells, as well as less active, more stationary cells, respectively.

In both energized and deenergized conditions, the final intracellular FLC concentration was higher in the $\Delta Cgip1$ strain (Figure 5E). In energized conditions, the $\Delta Cgip1$ strain accumulated significantly more fluconazole as early as 3 h post-treatment and continued to accumulate significantly more FLC compared to WT over the course of 24 h. In deenergized conditions, the $\Delta Cgip1$ strain accumulated higher fluconazole than the WT strain by the 8-h timepoint, but did not have significantly different intracellular FLC from WT until the 24-h post-treatment time point.

3.8. $\Delta Cgip1$ Cells Show Attenuated Virulence in Mouse Model

To assess whether the deletion of CgIp1 alters virulence, we used the neutropenic murine model of systemic candidiasis [49]. Neutropenic BALB/c mice were injected once used to assay kidney fungal burden by injecting them with WT, $\Delta Cgip1$ and $\Delta Cgip1::IPT1$ strains as described in Materials and Methods. Colonization (CFU/g) of kidneys for each strain at 24 to 48 h post-infection was determined by routine CFU determination procedures. Interestingly, the $\Delta Cgip1$ strain showed a significant decrease in CFU counts compared to the WT parental strain at 48 h post-infection (Figure 6). The $\Delta Cgip1::IPT1$ showed recovery of CFU counts at 48 h post-infection (Figure 6). Reduction of kidney burden in the mouse model suggests a role for CgIp1 in the virulence and pathogenicity mechanisms of *C. glabrata*.

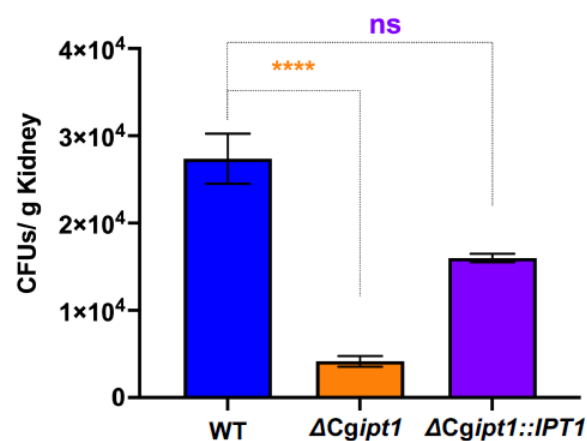


Figure 6. $\Delta Cgip1$ cells show reduced fungal burden in vivo. $\Delta Cgip1$ cells show reduced fungal burden in kidney. CFU recovered from kidney were significantly low in $\Delta Cgip1$ cells as compared with the WT cells as mentioned in the indicated time points. Significant differences at CFU levels are indicated as **** $p < 0.0001$; ns, not significantly different calculated using Student's *t*-test on graph pad prism 9.

4. Discussion

Past studies have underscored the relevance of SLs in influencing physiological processes in yeast cells. Not only do these molecules provide signaling cues to impact virulence of *C. albicans* cells, but their imbalanced lipid homeostasis also affects membrane protein cellular trafficking and drug susceptibility. The inherent structural peculiarities of acidic SLs in yeast (the absence of inositolphosphorylceramides in mammals) make them novel

drug targets, and hence justifiably continue to draw research attention. The present study has explored the hitherto unknown nature of inositolphosphorylceramides metabolism in *C. glabrata*, which is the second leading cause of human fungal infection after *C. albicans*. We selected two ORFs, CAGL0G05313g (CgIpt1) and CAGL0I10054g (CgSkn1), from the *C. glabrata* genome, which, based on their close homology with *S. cerevisiae* counterparts, are predicted to encode for inositol phosphoryl transferases. The successful single (Δ Cgipt1 and Δ Cgskn1) and double deletion (Cgipt1/Cgskn1 $\Delta\Delta$) of CgIpt1 and CgSkn1 confirmed the non-essential nature of the two homologues which contrasts with their indispensability in the budding yeast *S. cerevisiae*. The deletion of Δ Cgipt1 or Δ Cgskn1 in *C. glabrata* did not impact cellular growth of the cells implying that the loss of either of the two genes did not impose any fitness cost.

High throughput lipidomics of the parental strain compared to the two single-deletant strains (Δ Cgipt1 and Δ Cgskn1) revealed interesting insights into the physiological relevance of CgIpt1 and CgSkn1. The quantitation of IPC intermediate levels indicated that the ORF putatively encoding CgIpt1 is a major player of inositolphosphorylceramides transferase activity, wherein CgSkn1 probably has a minor role in IPC metabolism in *C. glabrata* cells. This is well supported by the fact that Δ Cgipt1 cells exhibited a strong phenotype reflected in an increased drug susceptibility to tested azoles while the susceptibility of Δ Cgskn1 cells towards azoles remained unchanged from the parental strain. The dominance of CgIpt1 in influencing drug susceptibility was further evident by increased susceptibility towards azoles observed in the Cgipt1/Cgskn1 $\Delta\Delta$ strain compared to the Δ Cgskn1 strain.

The role of yeast SL genes has been established in fundamental pathways like endocytosis, GPI-anchored proteins and vesicular trafficking, which are required for cell wall synthesis where the mutant genes were observed to show increased susceptibility on cell wall perturbing agents such as calcofluor white and SDS along with specific alteration in cell wall properties [61–64]. In our finding, the deletion of CgIpt1 did not impact the cell wall significantly (Figure S1B). The fact that Δ Cgipt1 cells have a structurally and functionally intact cell wall and yet present with a compromised plasma membrane is an interesting observation but is not surprising. One can argue that certain yeasts may have a cell wall defect but show no change in plasma membrane permeability. Furthermore, even if a cell shows resistance to cell wall perturbing agents, the overall cell permeability could still be altered [65].

Notably, the content of sterol and its intermediates were significantly higher in the Δ Cgipt1 strain compared to the parental strain. While an increase in ergosterol levels is commonly linked to enhanced resistance towards azoles in yeasts, this was not the case in the *C. glabrata* IPT1 mutant. Even with a high level of ergosterol in Δ Cgipt1, the mutant showed increased susceptibility to azoles, implying that imbalances in SLs alone can influence drug susceptibility in *C. glabrata*. This does not fit the usual convenient notion where azole susceptibility can be easily pinned on low ergosterol content and accumulation of branched “toxic” sterol intermediates [66]. Considering the fact that Δ Cgipt1 cells are trying to compensate for the loss of M(IP)₂C, by subtle changes in other lipid species composition, one could speculate that since M(IP)₂C structures in fungal membranes are mostly composed of hydroxylated very-long-chain fatty acid (VLCFA) [67], these structures can directly affect the order of the membrane. In this light, depletion of M(IP)₂C structures in the Δ Cgipt1 cell membrane could result in reduced membrane order, which in turn could be compensated by an increase in the content of specific sterol structures. In fact, in a specific study in *S. cerevisiae*, it was shown that IPT1 deletion strongly affects the rigidity of gel domains without influencing their relative abundance, whereas no significant alterations could be perceived in ergosterol-enriched domains [68]. In a separate study in *C. albicans*, we have shown that deletion of IPT1 destabilizes the membrane microdomains which in turn impairs the functionality of Cdr1, which is a major fluconazole efflux pump [20]. Therefore, it would not be wrong to presume that deletant of IPT1 in *C. glabrata*: accumulates MIPC in the membrane, has low M(IP)₂C which is balanced by increase in sterol structures, local membrane micro-environment is altered in such a

way that promotes higher drug diffusion and drug efflux pumps are thereby rendered defunct, leading to increased azole susceptibility of $\Delta CgIpt1$ cells. Although specific sterol structures and altered membrane microdomain could directly affect the functionality of the protein localized therein [69], some of which may be directly linked to azole resistance. However, another study in *C. albicans* cells described a different mechanism for azole susceptibility [70]. Zhang et al. argue that the reduction of ergosterol upon fluconazole treatment of *C. albicans* impairs vacuolar acidification, whereas concomitant ergosterol feeding restored V-ATPase function and cell growth. In *C. glabrata* there is a possibility that the plasma membrane of $\Delta CgIpt1$ cells accumulates certain sterol structures that disrupt the membrane order, or there may be some other mechanism could be involved. There are also reports on *C. glabrata* which do not find a direct correlation between increased sterols and enhanced susceptibility to fluconazole [71–73]. No major differences were noted in the level of expression of *ERG* genes between drug resistant and susceptible isolates [74,75], implying no direct link between increased azole resistance and overexpression of *CgERG* genes [76].

It was observed that the lipid imbalances caused by the *CgIpt1* gene deletion led to an increase in membrane fluidity (revealed by FRAP measurements). This was supported by increased drug uptake (indicated by increased intracellular ^3H -FLC accumulation) in the $\Delta CgIpt1$ strain compared to its parent WT strain. Increased membrane fluidity, allowing more drug into the cells, could contribute to the increased drug susceptibility (revealed by broth drug microdilution) of the $\Delta CgIpt1$ strain (Figure 7). Together, we report the first functional characterization of two putative inositolphosphoryltransferase-encoding ORFs of *C. glabrata* genome. We show that among the two homologs, CAGL0G05313g (*CgIpt1*) is a major inositolphosphoryltransferase which influences drug susceptibility and virulence of *C. glabrata*, while its close homologue CAGL0I10054g (*CgSkn1*) does not appear to be a major contributor of IPC metabolism and its functional relevance remains to be explored.

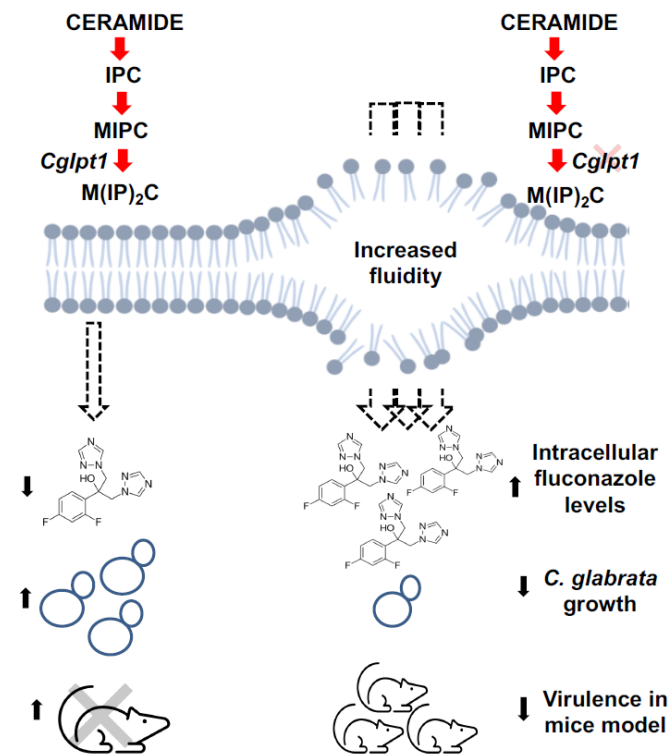


Figure 7. Model depicting the impact of *CgIpt1* deletion on *C. glabrata* cells. The deletion of the gene results in imbalances in SL homeostasis and consequently an increased membrane fluidity, which further leads to an enhanced diffusion of the antifungal FLC. The resulting increased intracellular FLC increases FLC susceptibility, impedes cellular growth and compromises the virulence of *C. glabrata* in a mouse model.

Supplementary Materials: The following are available online at <https://www.mdpi.com/article/10.3390/jof8070651/s1>, Figure S1: Drug susceptibility analysis of WT, $\Delta Cgip1$ and $\Delta Cgip1::IPT1$ strains using the spot assay. (A-B) Drug susceptibility to KTZ, MCZ, CTZ, FLC, ITR and PCZ and other xenobiotics was determined by spot assay.; Figure S2. Drug susceptibility analysis of WT and $\Delta Cgskn1$ strains. Drug susceptibility was determined by spot assay.; Figure S3. PCA analysis of lipid species dataset of WT and $\Delta Cgip1$. (A) Principal components 1 and 2 account for as much as 88% variance in the datasets. (B) PCA loading plot representing the contribution to individual lipid species to the overall variance is shown. Table S1: List of strains used in the study, Supplementary Sheet S1: Comparative lipidomic data of WT, $\Delta Cgip1$ and $\Delta Cgskn1$ strains. Data represented in nmol per mg lipid dry wt (n = 3).

Author Contributions: Conceptualization, A.S. and R.P.; Data curation, G.S., M.K., N.K.K., A.B., A.S. and R.P.; Formal analysis, G.S., M.K. and N.K.K.; Funding acquisition, N.A.G., A.S. and R.P.; Methodology, G.S., M.K., N.K.K., A.B., P.S., S.K., B.D.E., N.C., A.C., T.C.W. and A.S.; Supervision, A.S. and R.P.; Writing—original draft, G.S. and A.S.; Writing—review and editing, A.S. and R.P. All authors have read and agreed to the published version of the manuscript.

Funding: RP acknowledges support from ICMR (AMR/149 (2)-2018-ECD-II), RP, AS and AB from DBT (BT/PR38505/MED/29/1513/2020). AS thanks support from ICMR (No.52/08/2019-BIO/BMS), DST-PURSE program (SR/PURSE Phase 2/29©), UP Higher Education (No. 10/2021/281/-4-Sattar-2021-04(2)/2021), and the University of Lucknow. NAG acknowledges ICGB, New Delhi, and Department of Biotechnology (DBT), Government of India for financial support (Grant No.: BT/PB/Centre/03/ICGB/2011-PhaseII). APC was covered by the Journal of Fungi Editorial Office.

Institutional Review Board Statement: The animal studies described herein were compliant with the provisions established by the Animal Welfare Act (AWA) and the Public Health Services (PHS) policy on the humane care and use of laboratory animals. All animal experiments were performed in accordance with the Rutgers University Institutional Animal Care and Use Committee (IACUC) approved animal protocol.

Informed Consent Statement: Not applicable.

Data Availability Statement: Not applicable.

Acknowledgments: The lipid analyses described in this work were performed in parts at the Kansas Lipidomics Research Center Analytical Laboratory, Kansas State University, USA (funded by NSF grants EPS 0236913, MCB 1413036, MCB 0920663, DBI 0521587, DBI1228622 and K-INBRE of NIH P20GM103418), The Amity Lipidomics Research Facility (ALRF), and Central Instrumental research Facility (CIRF). The support of Amity University Haryana, India is gratefully acknowledged.

Conflicts of Interest: The authors declare that no conflict of interest exist. The authors have no other relevant affiliations or financial involvement with any organization or entity with a financial interest in or financial conflict with the subject matter or materials discussed in the manuscript apart from those disclosed.

References

1. Brown, G.D.; Denning, D.W.; Gow, N.A.R.; Levitz, S.M.; Netea, M.G.; White, T.C. Hidden Killers: Human Fungal Infections. *Sci. Transl. Med.* **2012**, *4*, 165rv13. [[CrossRef](#)] [[PubMed](#)]
2. Prasad, R.; Nair, R.; Banerjee, A. Multidrug Transporters of Candida Species in Clinical Azole Resistance. *Fungal Genet. Biol.* **2019**, *132*, 103252. [[CrossRef](#)] [[PubMed](#)]
3. Mukhopadhyay, K.; Kohli, A.; Prasad, R. Drug Susceptibilities of Yeast Cells Are Affected by Membrane Lipid Composition. *Antimicrob. Agents Chemother.* **2002**, *46*, 3695–3705. [[CrossRef](#)] [[PubMed](#)]
4. Cowen, L.E.; Sanglard, D.; Howard, S.J.; Rogers, P.D.; Perlin, D.S. Mechanisms of Antifungal Drug Resistance. *Cold Spring Harb. Perspect. Med.* **2014**, *5*, a019752. [[CrossRef](#)] [[PubMed](#)]
5. Kohli, A.; Smriti; Mukhopadhyay, K.; Rattan, A.; Prasad, R. In Vitro Low-Level Resistance to Azoles in Candida Albicans Is Associated with Changes in Membrane Lipid Fluidity and Asymmetry. *Antimicrob. Agents Chemother.* **2002**, *46*, 1046–1052. [[CrossRef](#)] [[PubMed](#)]
6. Prasad, R.; Singh, A. Lipids of Candida Albicans and Their Role in Multidrug Resistance. *Curr. Genet.* **2013**, *59*, 243–250. [[CrossRef](#)] [[PubMed](#)]
7. Singh, A.; Prasad, R. Comparative Lipidomics of Azole Sensitive and Resistant Clinical Isolates of Candida Albicans Reveals Unexpected Diversity in Molecular Lipid Imprints. *PLoS ONE* **2011**, *6*, e19266. [[CrossRef](#)]

8. Rella, A.; Farnoud, A.M.; Del Poeta, M. Plasma Membrane Lipids and Their Role in Fungal Virulence. *Prog. Lipid Res.* **2016**, *61*, 63–72. [[CrossRef](#)] [[PubMed](#)]
9. Lattif, A.A.; Mukherjee, P.K.; Chandra, J.; Roth, M.R.; Welti, R.; Rouabhia, M.; Ghannoum, M.A. Lipidomics of Candida Albicans Biofilms Reveals Phase-Dependent Production of Phospholipid Molecular Classes and Role for Lipid Rafts in Biofilm Formation. *Microbiology* **2011**, *157 Pt 11*, 3232–3242. [[CrossRef](#)]
10. Jenkins, G.M.; Richards, A.; Wahl, T.; Mao, C.; Obeid, L.; Hannun, Y. Involvement of Yeast Sphingolipids in the Heat Stress Response of Saccharomyces Cerevisiae. *J. Biol. Chem.* **1997**, *272*, 32566–32572. [[CrossRef](#)]
11. Patton, J.L.; Srinivasan, B.; Dickson, R.C.; Lester, R.L. Phenotypes of Sphingolipid-Dependent Strains of Saccharomyces Cerevisiae. *J. Bacteriol.* **1992**, *174*, 7180–7184. [[CrossRef](#)] [[PubMed](#)]
12. Zanolari, B.; Friant, S.; Funato, K.; Sütterlin, C.; Stevenson, B.J.; Riezman, H. Sphingoid Base Synthesis Requirement for Endocytosis in Saccharomyces Cerevisiae. *EMBO J.* **2000**, *19*, 2824–2833. [[CrossRef](#)] [[PubMed](#)]
13. Obeid, L.M.; Okamoto, Y.; Mao, C. Yeast Sphingolipids: Metabolism and Biology. *Biochim. Biophys. Acta (BBA) Mol. Cell Biol. Lipids* **2002**, *1585*, 163–171. [[CrossRef](#)]
14. Cheng, J.; Park, T.-S.; Chio, L.-C.; Fischl, A.S.; Ye, X.S. Induction of Apoptosis by Sphingoid Long-Chain Bases in Aspergillus Nidulans. *Mol. Cell Biol.* **2003**, *23*, 163–177. [[CrossRef](#)]
15. Luberto, C.; Toffaletti, D.L.; Wills, E.A.; Tucker, S.C.; Casadevall, A.; Perfect, J.R.; Hannun, Y.A.; Del Poeta, M. Roles for Inositol-Phosphoryl Ceramide Synthase 1 (IPC1) in Pathogenesis of C. Neoformans. *Genes Dev.* **2001**, *15*, 201–212. [[CrossRef](#)] [[PubMed](#)]
16. Epstein, S.; Castillon, G.A.; Qin, Y.; Riezman, H. An Essential Function of Sphingolipids in Yeast Cell Division. *Mol. Microbiol.* **2012**, *84*, 1018–1032. [[CrossRef](#)]
17. Mukhopadhyay, K.; Prasad, T.; Saini, P.; Pucadyil, T.J.; Chattopadhyay, A.; Prasad, R. Membrane Sphingolipid-Ergosterol Interactions Are Important Determinants of Multidrug Resistance in Candida Albicans. *Antimicrob. Agents Chemother.* **2004**, *48*, 1778–1787. [[CrossRef](#)]
18. Pasrija, R.; Prasad, T.; Prasad, R. Membrane Raft Lipid Constituents Affect Drug Susceptibilities of Candida Albicans. *Biochem. Soc. Trans.* **2005**, *33*, 1219–1223. [[CrossRef](#)]
19. Pasrija, R.; Panwar, S.L.; Prasad, R. Multidrug Transporters CaCdr1p and CaMdr1p of Candida Albicans Display Different Lipid Specificities: Both Ergosterol and Sphingolipids Are Essential for Targeting of CaCdr1p to Membrane Rafts. *Antimicrob. Agents Chemother.* **2008**, *52*, 694–704. [[CrossRef](#)]
20. Prasad, T.; Saini, P.; Gaur, N.A.; Vishwakarma, R.A.; Khan, L.A.; Haq, Q.M.R.; Prasad, R. Functional Analysis of CaIPT1, a Sphingolipid Biosynthetic Gene Involved in Multidrug Resistance and Morphogenesis of Candida Albicans. *Antimicrob. Agents Chemother.* **2005**, *49*, 3442–3452. [[CrossRef](#)]
21. Martin, S.W.; Konopka, J.B. Lipid Raft Polarization Contributes to Hyphal Growth in Candida Albicans. *Eukaryot. Cell* **2004**, *3*, 675–684. [[CrossRef](#)] [[PubMed](#)]
22. Mor, V.; Rella, A.; Farnoud, A.M.; Singh, A.; Munshi, M.; Bryan, A.; Naseem, S.; Konopka, J.B.; Ojima, I.; Bullesbach, E.; et al. Identification of a New Class of Antifungals Targeting the Synthesis of Fungal Sphingolipids. *mBio* **2015**, *6*, e00647. [[CrossRef](#)]
23. Pfaller, M.A.; Diekema, D.J. Epidemiology of Invasive Candidiasis: A Persistent Public Health Problem. *Clin. Microbiol. Rev.* **2007**, *20*, 133–163. [[CrossRef](#)] [[PubMed](#)]
24. Guinea, J. Global Trends in the Distribution of Candida Species Causing Candidemia. *Clin. Microbiol. Infect.* **2014**, *20*, 5–10. [[CrossRef](#)] [[PubMed](#)]
25. Sanguinetti, M.; Posteraro, B.; Lass-Flörl, C. Antifungal Drug Resistance among Candida Species: Mechanisms and Clinical Impact. *Mycoses* **2015**, *58* (Suppl. S2), 2–13. [[CrossRef](#)]
26. Kołaczowska, A.; Kołaczkowski, M. Drug Resistance Mechanisms and Their Regulation in Non-Albicans Candida Species. *J. Antimicrob. Chemother.* **2016**, *71*, 1438–1450. [[CrossRef](#)]
27. vanden Bossche, H.; Marichal, P.; Odds, F.C.; Le Jeune, L.; Coene, M.C. Characterization of an Azole-Resistant Candida Glabrata Isolate. *Antimicrob. Agents Chemother.* **1992**, *36*, 2602–2610. [[CrossRef](#)]
28. Sanglard, D.; Ischer, F.; Calabrese, D.; Majcherczyk, P.A.; Bille, J. The ATP Binding Cassette Transporter Gene CgCDR1 from Candida Glabrata Is Involved in the Resistance of Clinical Isolates to Azole Antifungal Agents. *Antimicrob. Agents Chemother.* **1999**, *43*, 2753–2765. [[CrossRef](#)]
29. Costa, C.; Nunes, J.; Henriques, A.; Mira, N.P.; Nakayama, H.; Chibana, H.; Teixeira, M.C. Candida Glabrata Drug:H⁺ Antiporter CgTpo3 (ORF CAGL0110384g): Role in Azole Drug Resistance and Polyamine Homeostasis. *J. Antimicrob. Chemother.* **2014**, *69*, 1767–1776. [[CrossRef](#)]
30. Ferrari, S.; Ischer, F.; Calabrese, D.; Posteraro, B.; Sanguinetti, M.; Fadda, G.; Rohde, B.; Bauser, C.; Bader, O.; Sanglard, D. Gain of Function Mutations in CgPDR1 of Candida Glabrata Not Only Mediate Antifungal Resistance but Also Enhance Virulence. *PLoS Pathog.* **2009**, *5*, e1000268. [[CrossRef](#)] [[PubMed](#)]
31. Costa, C.; Pires, C.; Cabrito, T.R.; Renaudin, A.; Ohno, M.; Chibana, H.; Sá-Correia, I.; Teixeira, M.C. Candida Glabrata Drug:H⁺ Antiporter CgQdr2 Confers Imidazole Drug Resistance, Being Activated by Transcription Factor CgPdr1. *Antimicrob. Agents Chemother.* **2013**, *57*, 3159–3167. [[CrossRef](#)] [[PubMed](#)]
32. Paul, S.; Schmidt, J.A.; Moye-Rowley, W.S. Regulation of the CgPdr1 Transcription Factor from the Pathogen Candida Glabrata. *Eukaryot. Cell* **2011**, *10*, 187–197. [[CrossRef](#)] [[PubMed](#)]

33. Frías-De-León, M.G.; Hernández-Castro, R.; Conde-Cuevas, E.; García-Coronel, I.H.; Vázquez-Aceituno, V.A.; Soriano-Ursúa, M.A.; Farfán-García, E.D.; Ocharán-Hernández, E.; Rodríguez-Cerdeira, C.; Arenas, R.; et al. Candida Glabrata Antifungal Resistance and Virulence Factors, a Perfect Pathogenic Combination. *Pharmaceutics* **2021**, *13*, 1529. [[CrossRef](#)] [[PubMed](#)]
34. Filler, E.E.; Liu, Y.; Solis, N.V.; Wang, L.; Diaz, L.F.; Edwards, J.E.; Filler, S.G.; Yeaman, M.R.; Noverr, M.C. Identification of Candida Glabrata Transcriptional Regulators That Govern Stress Resistance and Virulence. *Infect. Immun.* **2021**, *89*, e00146-20. [[CrossRef](#)]
35. Vermitsky, J.-P.; Earhart, K.D.; Smith, W.L.; Homayouni, R.; Edlind, T.D.; Rogers, P.D. Pdr1 Regulates Multidrug Resistance in Candida Glabrata: Gene Disruption and Genome-Wide Expression Studies. *Mol. Microbiol.* **2006**, *61*, 704–722. [[CrossRef](#)]
36. Simonicova, L.; Moye-Rowley, W.S. Functional Information from Clinically-Derived Drug Resistant Forms of the Candida Glabrata Pdr1 Transcription Factor. *PLoS Genet.* **2020**, *16*, e1009005. [[CrossRef](#)]
37. Roetzer, A.; Gabaldón, T.; Schüller, C. From Saccharomyces Cerevisiae to Candida Glabrata in a Few Easy Steps: Important Adaptations for an Opportunistic Pathogen. *FEMS Microbiol. Lett.* **2011**, *314*, 1–9. [[CrossRef](#)]
38. Rai, M.N.; Balusu, S.; Gorityala, N.; Dandu, L.; Kaur, R. Functional Genomic Analysis of Candida Glabrata-Macrophage Interaction: Role of Chromatin Remodeling in Virulence. *PLoS Pathog.* **2012**, *8*, e1002863. [[CrossRef](#)]
39. Bialková, A.; Šubík, J. Biology of the Pathogenic Yeast Candida Glabrata. *Folia Microbiol.* **2006**, *51*, 3–20. [[CrossRef](#)]
40. Kumari, S.; Kumar, M.; Khandelwal, N.K.; Pandey, A.K.; Bhakt, P.; Kaur, R.; Prasad, R.; Gaur, N.A. A Homologous Overexpression System to Study Roles of Drug Transporters in Candida Glabrata. *FEMS Yeast Res.* **2020**, *20*, foaa032. [[CrossRef](#)]
41. Folch, J.; Lees, M.; Stanley, G.H.S. A Simple Method for the Isolation and Purification of Total Lipides from Animal Tissues. *J. Biol. Chem.* **1957**, *226*, 497–509. [[CrossRef](#)]
42. Singh, A.; Prasad, T.; Kapoor, K.; Mandal, A.; Roth, M.; Welti, R.; Prasad, R. Phospholipidome of Candida: Each Species of Candida Has Distinctive Phospholipid Molecular Species. *OMICS J. Integr. Biol.* **2010**, *14*, 665–677. [[CrossRef](#)] [[PubMed](#)]
43. Singh, A.; Yadav, V.; Prasad, R. Comparative Lipidomics in Clinical Isolates of Candida Albicans Reveal Crosstalk between Mitochondria, Cell Wall Integrity and Azole Resistance. *PLoS ONE* **2012**, *7*, e39812. [[CrossRef](#)] [[PubMed](#)]
44. Mahto, K.K.; Singh, A.; Khandelwal, N.K.; Bhardwaj, N.; Jha, J.; Prasad, R. An Assessment of Growth Media Enrichment on Lipid Metabolome and the Concurrent Phenotypic Properties of Candida Albicans. *PLoS ONE* **2014**, *9*, e113664. [[CrossRef](#)] [[PubMed](#)]
45. Kumari, S.; Kumar, M.; Esquivel, B.D.; Wasi, M.; Pandey, A.K.; Kumar, K.N.; Mondal, A.K.; White, T.C.; Prasad, R.; Gaur, N.A. Unmasking of CgYor1-Dependent Azole Resistance Mediated by Target of Rapamycin (TOR) and Calcineurin Signaling in Candida Glabrata. *mBio* **2022**, *13*, e03545-21. [[CrossRef](#)]
46. Esquivel, B.D.; Smith, A.R.; Zavrel, M.; White, T.C. Azole Drug Import into the Pathogenic Fungus Aspergillus Fumigatus. *Antimicrob. Agents Chemother.* **2015**, *59*, 3390–3398. [[CrossRef](#)]
47. Mansfield, B.E.; Oltean, H.N.; Oliver, B.G.; Hoot, S.J.; Leyde, S.E.; Hedstrom, L.; White, T.C. Azole Drugs Are Imported by Facilitated Diffusion in Candida Albicans and Other Pathogenic Fungi. *PLoS Pathog.* **2010**, *6*, e1001126. [[CrossRef](#)]
48. Koppel, D.E.; Sheetz, M.P.; Schindler, M. Lateral Diffusion in Biological Membranes. A Normal-Mode Analysis of Diffusion on a Spherical Surface. *Biophys. J.* **1980**, *30*, 187–192. [[CrossRef](#)]
49. Andes, D.R.; Diekema, D.J.; Pfaller, M.A.; Marchillo, K.; Bohrmueller, J. In Vivo Pharmacodynamic Target Investigation for Micafungin against Candida Albicans and C. Glabrata in a Neutropenic Murine Candidiasis Model. *Antimicrob. Agents Chemother.* **2008**, *52*, 3497–3503. [[CrossRef](#)]
50. Dickson, R.C.; Nagiec, E.E.; Wells, G.B.; Nagiec, M.M.; Lester, R.L. Synthesis of Mannose-(Inositol-P)2-Ceramide, the Major Sphingolipid in Saccharomyces Cerevisiae, Requires the IPT1 (YDR072c) Gene. *J. Biol. Chem.* **1997**, *272*, 29620–29625. [[CrossRef](#)]
51. Thevissen, K.; Idkowiak-Baldys, J.; Im, Y.-J.; Takemoto, J.; François, I.E.J.A.; Ferket, K.K.A.; Aerts, A.M.; Meert, E.M.K.; Winderickx, J.; Roosen, J.; et al. SKN1, a Novel Plant Defensin-Sensitivity Gene in Saccharomyces Cerevisiae, Is Implicated in Sphingolipid Biosynthesis. *FEBS Lett.* **2005**, *579*, 1973–1977. [[CrossRef](#)] [[PubMed](#)]
52. Thevissen, K.; Yen, W.-L.; Carmona-Gutierrez, D.; Idkowiak-Baldys, J.; Aerts, A.M.; François, I.E.J.A.; Madeo, F.; Klionsky, D.J.; Hannun, Y.A.; Cammue, B.P.A. Skn1 and Ipt1 Negatively Regulate Autophagy in Saccharomyces Cerevisiae. *FEMS Microbiol. Lett.* **2010**, *303*, 163–168. [[CrossRef](#)] [[PubMed](#)]
53. Roemer, T.; Delaney, S.; Bussey, H. SKN1 and KRE6 Define a Pair of Functional Homologs Encoding Putative Membrane Proteins Involved in Beta-Glucan Synthesis. *Mol. Cell. Biol.* **1993**, *13*, 4039–4048. [[CrossRef](#)] [[PubMed](#)]
54. Han, Q.; Wang, N.; Yao, G.; Mu, C.; Wang, Y.; Sang, J. Blocking β -1,6-Glucan Synthesis by Deleting KRE6 and SKN1 Attenuates the Virulence of Candida Albicans. *Mol. Microbiol.* **2019**, *111*, 604–620. [[CrossRef](#)]
55. Kurita, T.; Noda, Y.; Yoda, K. Action of Multiple Endoplasmic Reticulum Chaperon-like Proteins Is Required for Proper Folding and Polarized Localization of Kre6 Protein Essential in Yeast Cell Wall β -1,6-Glucan Synthesis. *J. Biol. Chem.* **2012**, *287*, 17415–17424. [[CrossRef](#)]
56. Moffett, S.; Brown, D.A.; Linder, M.E. Lipid-Dependent Targeting of G Proteins into Rafts. *J. Biol. Chem.* **2000**, *275*, 2191–2198. [[CrossRef](#)]
57. Prasad, T.; Chandra, A.; Mukhopadhyay, C.K.; Prasad, R. Unexpected Link between Iron and Drug Resistance of Candida Spp.: Iron Depletion Enhances Membrane Fluidity and Drug Diffusion, Leading to Drug-Susceptible Cells. *Antimicrob. Agents Chemother.* **2006**, *50*, 3597–3606. [[CrossRef](#)]
58. Dawaliby, R.; Trubbia, C.; Delporte, C.; Noyon, C.; Ruysschaert, J.-M.; Van Antwerpen, P.; Govaerts, C. Phosphatidylethanolamine Is a Key Regulator of Membrane Fluidity in Eukaryotic Cells. *J. Biol. Chem.* **2016**, *291*, 3658–3667. [[CrossRef](#)]

59. Galocha, M.; Costa, I.V.; Teixeira, M.C. Carrier-Mediated Drug Uptake in Fungal Pathogens. *Genes* **2020**, *11*, 1324. [[CrossRef](#)]
60. Esquivel, B.D.; White, T.C. Accumulation of Azole Drugs in the Fungal Plant Pathogen Magnaporthe Oryzae Is the Result of Facilitated Diffusion Influx. *Front. Microbiol.* **2017**, *8*, 1320. [[CrossRef](#)]
61. Pagé, N.; Gérard-Vincent, M.; Ménard, P.; Beaulieu, M.; Azuma, M.; Dijkgraaf, G.J.P.; Li, H.; Marcoux, J.; Nguyen, T.; Dowse, T.; et al. A Saccharomyces Cerevisiae Genome-Wide Mutant Screen for Altered Sensitivity to K1 Killer Toxin. *Genetics* **2003**, *163*, 875–894. [[CrossRef](#)] [[PubMed](#)]
62. Ragni, E.; Piberger, H.; Neupert, C.; García-Cantalejo, J.; Popolo, L.; Arroyo, J.; Aebi, M.; Strahl, S. The Genetic Interaction Network of CCW12, a Saccharomyces Cerevisiae Gene Required for Cell Wall Integrity during Budding and Formation of Mating Projections. *BMC Genom.* **2011**, *12*, 107. [[CrossRef](#)] [[PubMed](#)]
63. El-Sherbeini, M.; Clemas, J.A. Cloning and Characterization of GNS1: A Saccharomyces Cerevisiae Gene Involved in Synthesis of 1,3-Beta-Glucan in Vitro. *J. Bacteriol.* **1995**, *177*, 3227–3234. [[CrossRef](#)] [[PubMed](#)]
64. de Groot, P.W.J.; Ruiz, C.; Vázquez de Aldana, C.R.; Duenas, E.; Cid, V.J.; Del Rey, F.; Rodríguez-Peña, J.M.; Pérez, P.; Andel, A.; Caubín, J.; et al. A Genomic Approach for the Identification and Classification of Genes Involved in Cell Wall Formation and Its Regulation in Saccharomyces Cerevisiae. *Comp. Funct. Genom.* **1900**, *2*, 349784. [[CrossRef](#)]
65. Campodónico, V.L.; Rifat, D.; Chuang, Y.-M.; Ioerger, T.R.; Karakousis, P.C. Altered Mycobacterium Tuberculosis Cell Wall Metabolism and Physiology Associated With RpoB Mutation H526D. *Front. Microbiol.* **2018**, *9*, 494. [[CrossRef](#)]
66. Lan, Q.; Li, Y.; Wang, F.; Li, Z.; Gao, Y.; Lu, H.; Wang, Y.; Zhao, Z.; Deng, Z.; He, F.; et al. Deubiquitinase Ubp3 Enhances the Proteasomal Degradation of Key Enzymes in Sterol Homeostasis. *J. Biol. Chem.* **2021**, *296*, 100348. [[CrossRef](#)]
67. Ejsing, C.S.; Sampaio, J.L.; Surendranath, V.; Duchoslav, E.; Ekroos, K.; Klemm, R.W.; Simons, K.; Shevchenko, A. Global Analysis of the Yeast Lipidome by Quantitative Shotgun Mass Spectrometry. *Proc. Natl. Acad. Sci. USA* **2009**, *106*, 2136–2141. [[CrossRef](#)]
68. Bento-Oliveira, A.; Santos, F.C.; Marquês, J.T.; Paulo, P.M.R.; Korte, T.; Herrmann, A.; Marinho, H.S.; de Almeida, R.F.M. Yeast Sphingolipid-Enriched Domains and Membrane Compartments in the Absence of Mannosyldiinositolphosphorylceramide. *Biomolecules* **2020**, *10*, 871. [[CrossRef](#)]
69. Kim, J.H.; Singh, A.; Del Poeta, M.; Brown, D.A.; London, E. The Effect of Sterol Structure upon Clathrin-Mediated and Clathrin-Independent Endocytosis. *J. Cell Sci.* **2017**, *130*, 2682–2695. [[CrossRef](#)]
70. Zhang, Y.-Q.; Gamarra, S.; Garcia-Effron, G.; Park, S.; Perlin, D.S.; Rao, R. Requirement for Ergosterol in V-ATPase Function Underlies Antifungal Activity of Azole Drugs. *PLoS Pathog.* **2010**, *6*, e1000939. [[CrossRef](#)]
71. Gomez-Lopez, A.; Buitrago, M.J.; Rodriguez-Tudela, J.L.; Cuenca-Estrella, M. In Vitro Antifungal Susceptibility Pattern and Ergosterol Content in Clinical Yeast Strains. *Rev. Iberoam. Micol.* **2011**, *28*, 100–103. [[CrossRef](#)] [[PubMed](#)]
72. Salazar, S.B.; Wang, C.; Münsterkötter, M.; Okamoto, M.; Takahashi-Nakaguchi, A.; Chibana, H.; Lopes, M.M.; Güldener, U.; Butler, G.; Mira, N.P. Comparative Genomic and Transcriptomic Analyses Unveil Novel Features of Azole Resistance and Adaptation to the Human Host in Candida Glabrata. *FEMS Yeast Res.* **2018**, *18*, fox079. [[CrossRef](#)] [[PubMed](#)]
73. Pais, P.; Galocha, M.; Viana, R.; Cavalheiro, M.; Pereira, D.; Teixeira, M.C. Microevolution of the Pathogenic Yeasts Candida Albicans and Candida Glabrata during Antifungal Therapy and Host Infection. *Microb. Cell* **2019**, *6*, 142–159. [[CrossRef](#)] [[PubMed](#)]
74. Tsai, H.F.; Sammons, L.R.; Zhang, X.; Suffis, S.D.; Su, Q.; Myers, T.G.; Marr, K.A.; Bennett, J.E. Microarray and Molecular Analyses of the Azole Resistance Mechanism in Candida Glabrata Oropharyngeal Isolates. *Antimicrob. Agents Chemother.* **2010**, *54*, 3308–3317. [[CrossRef](#)] [[PubMed](#)]
75. Hull, C.M.; Parker, J.E.; Bader, O.; Weig, M.; Gross, U.; Warrilow, A.G.S.; Kelly, D.E.; Kelly, S.L. Facultative Sterol Uptake in an Ergosterol-Deficient Clinical Isolate of Candida Glabrata Harboring a Missense Mutation in ERG11 and Exhibiting Cross-Resistance to Azoles and Amphotericin B. *Antimicrob. Agents Chemother.* **2012**, *56*, 4223–4232. [[CrossRef](#)]
76. Brun, S.; Bergès, T.; Poupard, P.; Vauzelle-Moreau, C.; Renier, G.; Chabasse, D.; Bouchara, J.-P. Mechanisms of Azole Resistance in Petite Mutants of Candida Glabrata. *Antimicrob. Agents Chemother.* **2004**, *48*, 1788–1796. [[CrossRef](#)] [[PubMed](#)]